IMA Journal of Mathematics Applied in Medicine and Biology (2002) **19**, 31–60

Fluid flow in the anterior chamber of a human eye

C. R. CANNING AND M. J. GREANEY

Southampton Eye Unit, Southampton General Hospital, Tremona Road, Southampton, SO16 6YD, UK

J. N. DEWYNNE

OCIAM, Mathematical Institute, 24–29 St Giles, Oxford OX1 3LB, UK

AND

A. D. FITT

Faculty of Mathematical Studies, University of Southampton, Southampton SO17 1BJ, UK

[Received on 10 January 2001; revised on 20 February 2002]

A simple model is presented to analyse fluid flow in the anterior chamber of a human eye. It is shown that under normal conditions such flow inevitably occurs. The flow, whose reduced Reynolds number is small, is viscosity dominated and is driven by buoyancy effects which are present because of the temperature difference between the front and back of the anterior chamber. In cases of severe eye trauma or as a result of certain diseases and medical conditions, particulate matter may be introduced into the anterior chamber The motion and distribution of such particles is analysed and it is shown that the model is capable of predicting well-established and observed features that may be present in a traumatized eye such as hyphemas, keratic precipitates, hypopyons and Krukenberg spindles.

Keywords: human eyes; buoyancy-driven flow hyphemas; hypopyon; Krukenberg spindle; asymptotic analysis.

1. Introduction

Eye surgeons have long recognized the importance of understanding the minutiae of processes occurring inside and around the eye. However, many aspects of fluid mechanics within the eye have not yet been fully examined or quantitatively explained. Our objective in this study is to examine, using simple standard fluid dynamical models, the details of clinically observed flow in the anterior chamber which is caused by thermal processes. We also aim to identify circumstances where such flow is relevant to various aspects of eye disease.

Figure 1 gives a basic idea of the geometry and structure of the eye. Broadly speaking, the front of the eye may be thought of as comprising two chambers, the anterior chamber (between the iris and the cornea) and the posterior chamber (the region behind the iris and anterior to the hyaloid membrane). A number of other important regions and components of the eye are also identified in the diagram.

© The Institute of Mathematics and its Applications 2002

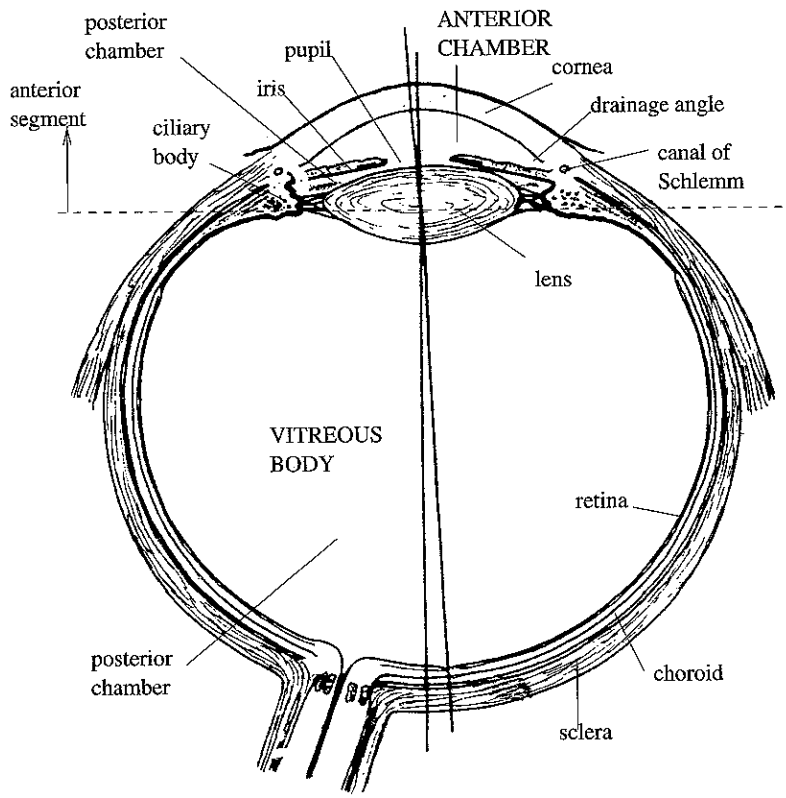

FIG 1 The main components of a human eye in horizontal cross-section.

Flow in the anterior chamber of the eye is a well known phenomenon that has been observed clinically. Ehrlich (1882) observed that systemic fluorescin (a water soluble yellow dye which, when injected into the body, leaks from the iris blood vessels so allowing flow visualization) tended to appear in the anterior chamber of animal eyes in a centrally placed vertical line. It was suggested in Türk (1906, 1911) that this phenomenon may result from fluid flow in the anterior chamber driven by a temperature gradient. Subsequently, the general idea of anterior chamber convection appears to have been adopted in the general literature. Although occasionally the subject has been revisited (see, for example, Wyatt (1996) who concluded that anterior chamber convection was responsible for asymmetries in pupil shape and placement during pharmacologic pupil dilation) to our knowledge no attempt has yet been made to carry out a systematic fluid mechanical analysis of the phenomenon.

Flow appears to take place in a single convection cell, rising (i.e. opposing gravity) near to the back of the chamber and falling towards the front. There seems to be little or no lateral movement of fluid. Although detailed experimental measurements do not yet appear to have been made, anecdotal flow transit times (the time taken for a fluid particle to move from the top to the bottom of the anterior chamber, say) of around one minute seem

normal. The fluid present in this part of the eye is produced continuously by the ciliary body. It flows through the pupil aperture in the centre of the back wall of the chamber. The fluid may be assumed to be a linear viscous fluid with a viscosity, density and expansivity identical to that of water. Fluid drains from the chamber through channels in the angle between the iris and the cornea (the 'drainage angle').

The observed flow is driven by buoyant convection arising from the temperature gradient that is present across the anterior chamber of the eye. This difference exists because the temperature at the back of the anterior chamber is close to core body temperature (37° C) whilst the outside of the cornea, which forms the front wall of the chamber, is exposed to ambient conditions (say 25° C during the day when the eye is open) The thickness of the cornea is typically 0·6 mm and its thermal insulation properties are likely to be similar to those of water. The temperature of the inner surface of the cornea is therefore likely to be quite close to 37° C. The principal aim of this study is to show that even relatively small temperature differences could give rise to the flows that are observed.

In isolation, the flow in the anterior chamber of the eye is not especially significant. It may assume greater importance, however, in cases where particulate matter is present in the anterior chamber. This may happen for a number of reasons: red or white blood cells may be present as a result of a variety of diseases or conditions and in other circumstances pigment particles may detach from the iris. Each different type of particulate matter may give rise to distinct symptoms and medical problems that require treatment. Below we give the basic details of the effects that each sort of particle may have.

1.1 *Red blood cells*

Red blood cells (erythrocytes) are not normally found in the anterior chamber of the eye. Their presence indicates rupture of one or more of the blood vessels in the eye. Red cells may exist in the anterior chamber in two forms.

(i) 'Fresh' red cells. These cells are normally less than 120 days old and retain their enzymatic machinery for energy metabolism. They are thus able to maintain a pliable cell membrane. Such cells have the form of plates, but can deform substantially when required to do so. This allows them to squeeze through the trabecular meshwork in the drainage angle with ease to clear rapidly from the anterior chamber. Fresh red blood cells may enter the anterior chamber via the pupil aperture or from rupture of a blood vessel within the chamber itself.

(ii) 'Ghost' cells. These cells are typically much more than 120 days old. They have lost their enzyme energy pathways and, due to membrane rupture, contain no haemoglobin The cell walls have thus become spherical and rigid. These cells are not able to deform to pass through the trabecular meshwork and tend to clog the drainage angle. Consequently, fluid is unable to escape from the chamber and the pressure within the eye rises, which may lead to blinding eye damage. Ghost cells always enter the anterior chamber through the pupil aperture from a source in the posterior segment. They tend not to adhere either to each other or to the walls of the chamber.

Detailed measurements of the density and size of erythrocytes are readily available in the the literature: for example, Weatherall *et al.* (1996) asserts that a red cell has a density that lies in the range 1092–1100 kg m^{-3} and a diameter of 6·7–7·7 μm. The density of an erythrocyte is given in Duck (1990) as 1089–1097 kg m^{-3} and in Lurie (1992) as 1090–

1106 kg m^{-3}, while Seeley *et al.* (2000) gives the diameter of a fresh red cell as 7·5 μm. We have however been unable to find comparable data for ghost cells. For the remainder of this study we assume for definiteness that the radius of a ghost cell is similar to a fresh red cell, and is given by 3·5 μm, but the density of a ghost cell is higher than the corresponding value for a fresh cell owing to cellular collapse and subsequent concentration. We therefore assume that the red cells that we shall be considering have a density of 1500 kg m^{-3}. It is worth pointing out that numerical experiments have confirmed that the details of the flows considered below are altered only by small amounts if a different value for red cell density is used.

Red blood cells may accumulate in large quantities and sediment to the bottom of the anterior chamber forming a layer known as a hyphema (see Fig. 2). One of the aims of formulating a quantitative mathematical model for aqueous humour flow in the anterior chamber is to determine whether such flow might disrupt a hyphema. Presumably if the flow is powerful enough then regions of a prospective hyphema cannot remain stationary. We shall show below that it is possible to calculate the theoretical maximum extent of a hyphema.

1.2 *White blood cells*

Leukocytes (white blood cells) may also be present in the anterior chamber of the eye. The presence of white blood cells normally indicates that the patient is suffering from uveitis (inflammation of the uveal tissues, and most importantly the ciliary body). This inflammation may lead to damage in the eye and sight loss.

During ophthalmic examination, white blood cells may be observed as so-called keratic precipitates (see Fig. 2). Each precipitate is a round aggregation of white cells, the aggregates typically being distributed in an approximately triangular shape. If these precipitates accumulate in sufficient quantities then a white layer similar to a hyphema may also form (a hypopyon).

The white blood cells present when uveitis occurs may be assumed to be spherical (see, for example, Caro *et al.*, 1978) and larger than the 'ghost' red blood cells described above; diameters of around 10 μm are typical (Seeley *et al.* (2000) gives diameter ranges of 10–12 μm (neutrophils), 10–12 μm (basophils), 11–14 μm (eosinophils), 6–14 μm (lymphocytes), 12–20 μm (monocytes) for various forms of leukocyte) and such cells will therefore be assumed for the remainder of this study to have a radius of 5 μm. The density of white cells appears to be similar to, but slightly less than, the density of fresh red cells. In the discussion below we concentrate on the formation of hyphemas and Krukenberg spindles. If one wished to perform detailed calculations of the formation of keratic precipitates and hypopyons, then the work of Cramer *et al.* (1992) suggests that a density of 1085·3 kg m^{-3} would be an appropriate value to use. It should also be noted that, in contrast to red cells, some white cells are 'sticky'. They may adhere to one another to form clumps and also (if they touch it) to the corneal endothelium (the inside surface of the cornea). Entry into the anterior chamber of white blood cells is usually from the front of the iris.

Optically, the sight of a patient is not usually affected by the presence of keratic precipitates. When diagnosed, however, they provide a clear indication that uveitis is present and treatment is normally required.

1.3 *Pigment particles*

Pigment provides a third type of particulate matter that might be present in the anterior chamber of the eye. Though complete pigment cells (melanocytes) are not usually released whole into the anterior chamber, melanin particles ('granules'), which are much smaller than blood cells, may be present in a variety of conditions (see, for example, Kuchle *et al.*, 1998 and Farrar & Shields, 1993). This presents us with a potential difficulty as there seems to a dearth of well-documented information concerning the size distribution and density of such particles. It is generally accepted that melanin granules are both much denser and much smaller than either red or white blood cells. For the remainder of this study we therefore assume that pigment particles have a density of $1700\,\mathrm{kg\,m^{-3}}$ and are spherical, with a diameter of $0{\cdot}5\,\mu\mathrm{m}$. Experience suggests that, unlike white blood cells, pigment particles do not easily adhere to each other. They do, however, possess some 'stickyness', and may become attached to the cornea under some circumstances.

Though pigment may be released from either the front or the back of the iris, it is known that most of the pigment present in the anterior chamber originates from the back of the iris and consequently enters the chamber through the pupil aperture. The diameter of the pupil aperture is not fixed, varying both with light conditions, focusing and age. In normal light conditions the aperture diameter is likely to be between 4 and 4·5 mm for a young person, this figure falling to 2 mm for an older subject. We therefore assume that the aperture may vary between 2 and 6 mm, the latter figure being achieved for a young patient in mainly dark surroundings.

Pigment particles may be released from the iris for a number of reasons, the two most common being associated with short-sightedness and diabetes. Pigment release may also occur after eye trauma (for example, if the eye has been struck by a foreign object), or in the presence of PDS (pigment dispersion syndrome), a condition that is genetic in its origins and is particularly prevalent in young males of Scandinavian origin.

From a diagnostic point of view, pigment can accumulate on the inner surface of the cornea, forming a so-called Krukenberg spindle (see Krukenberg, 1899) (see Fig. 2). Krukenberg spindles occur in a variety of positions on the cornea and may assume many shapes; often the greatest concentration of particles occurs at the centre of the cornea. Since the particle concentration by both weight and volume is very small, the patient's sight is not affected. However, the presence of a Krukenberg spindle is normally interpreted as a warning that the drainage mechanism of the eye may become slowly blocked. Some patients presenting with a Krukenberg spindle may consequently develop pigmentary glaucoma.

1.4 *Fluid flow in the vitreous body*

A number of reasons why flow in the anterior chamber may be important have been outlined above. Before concentrating solely on this region of the eye however, it is worth briefly mentioning that, under some (artificially induced) circumstances, thermally driven flow may also take place in the posterior segment of the eye.

The posterior part of the eye is normally filled with vitreous gel that is optically similar to water, being composed of about 99·9% H_2O. The remaining 0·1% is composed of a protein (present in long, thin strands), together with proteoglycans and GAGs

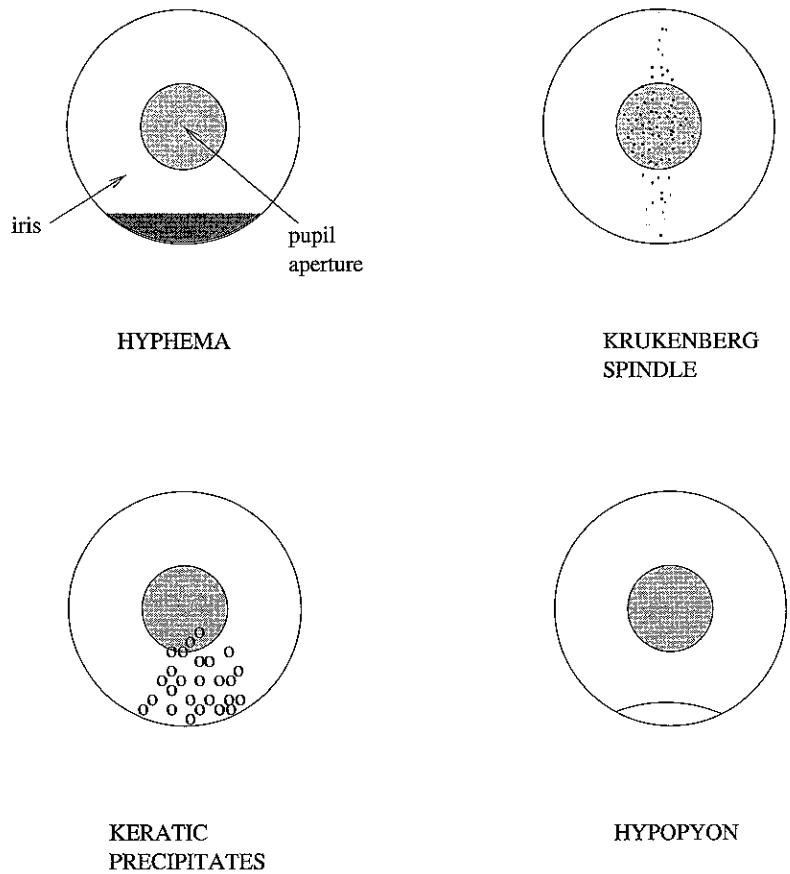

FIG 2. Schematic diagram of visual appearance of typical instances of hyphema, Krukenberg spindle, keratic precipitates and hypopyon (looking front on at the anterior chamber).

(glycosaminoglycans). This mixture plays a key role in determining the properties of the vitreous. Although the details are complicated (see, for example, Fatt & Weissman, 1992), the simplest model of the behaviour of the vitreous assumes that the large hydrodynamic resistance of the GAGs endows the gel with an effective yield stress. This prevents any bulk fluid flow in the gel under normal circumstances, though as the eye moves the gel may be shaken and elastic waves may propagate through it. In a variety of eye diseases and conditions (for example, retinal detachment) the gel needs to be removed (vitrectomy). Ultimately, the gel is replaced by the same type of fluid that is found in the anterior chamber. If a temperature difference exists between the front and back of the posterior segment then convection might also occur here. The existence of such convection currents is not widely accepted, although there is some supporting observational and anecdotal evidence. We are currently carrying out (mainly numerical) work on this aspect of flow in the eye; this will be addressed separately in another study

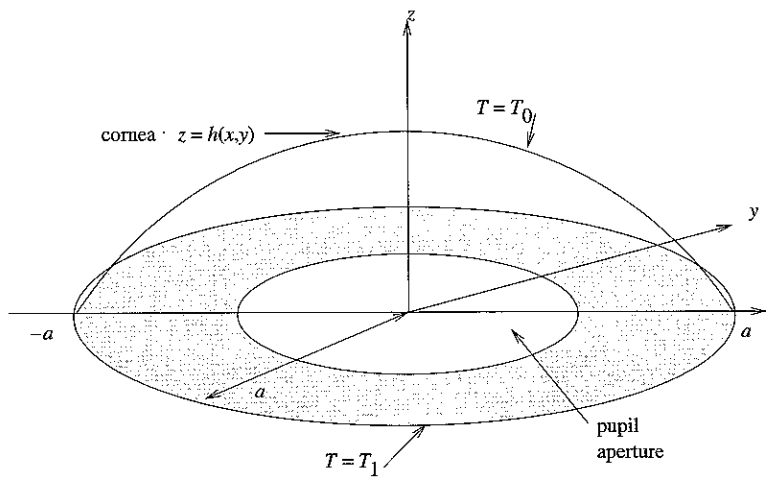

FIG 3 Schematic diagram of anterior chamber

We end this introductory section by reviewing our objectives. We aim to propose a simple fluid mechanics model which shows how, under normal conditions, flow in the anterior chamber inevitably takes place. The model should also be capable of predicting the formation of a hyphema or a Krukenberg spindle. (We omit specific consideration of the details of keratic precipitate and hypopyon formation.) Since obtaining qualitative and phenomenological information is our prime requirement we shall eschew large, purely numerical studies of the flow and use basic fluid mechanics and standard asymptotic analysis to examine the flow.

2. A model for thermally driven flow in the anterior chamber of the eye

We consider flow driven by thermal effects in the front portion of the eye between the cornea and the pupil. Figure 3 shows a schematic diagram of the flow that we wish to consider. We assume that fluid is contained between $z = 0$ and a solid (known) impermeable boundary at the cornea $z = h(x, y)$. This latter boundary is exposed to the elements and thus its temperature is held fixed at T_0, say. (As noted above, the cornea, which may be taken to have a constant thickness of 0 6 mm, insulates the anterior chamber from ambient conditions to some extent, and so the temperature difference that is perceived by the fluid in the anterior chamber will be reduced. T_0 should therefore be thought of as a 'given' constant rather than room temperature, for example) At the pupil/iris $z = 0$, the temperature is held fixed at T_1 which we consider to be close to body temperature and thus in excess of T_0. The patient is assumed to be in an upright position so that gravity acts along the positive x-axis.

According to the classical Boussinesq model (for details, see for example Drazin & Reid, 1981) for thermally driven convective flows, we assume that the fluid density ρ varies

slightly with temperature, but negligibly with pressure. Thus

$$\rho = \rho_0(1 - \alpha(T - T_0))$$

where T denotes temperature, ρ_0 is the fluid density at temperature T_0, and α is the coefficient of linear thermal expansion of the fluid (which we shall take to be given by the value for water at 30° C, namely $3 \times 10^{-4}\,\mathrm{K}^{-1}$ Batchelor, 1985). Because changes in the density are assumed to be small, the variable ρ may now be replaced everywhere by ρ_0, except when it appears in the gravity term. The governing equations of motion are thus

$$\rho_0(\boldsymbol{q}_t + (\boldsymbol{q}\ \nabla)\boldsymbol{q}) = -\nabla p + \rho_0 \nu \nabla^2 \boldsymbol{q} + \rho_0(1 - \alpha(T - T_0))\boldsymbol{g} \tag{2.1}$$

$$\nabla \cdot \boldsymbol{q} = 0 \tag{2.2}$$

$$T_t + (\boldsymbol{q}\ \nabla)T = \frac{k}{\rho_0 c_p}\nabla^2 T + \frac{1}{\rho_0 c_p}\Phi \tag{2.3}$$

$$\mathcal{D}c = 0. \tag{2.4}$$

Here the fluid velocity is denoted by $\boldsymbol{q} = u\hat{\boldsymbol{e}}_x + v\hat{\boldsymbol{e}}_y + w\hat{\boldsymbol{e}}_z$ where $\hat{\boldsymbol{e}}_x$, $\hat{\boldsymbol{e}}_y$ and $\hat{\boldsymbol{e}}_z$ are unit vectors in the x, y and z directions respectively. Subscripts denote derivatives, p denotes pressure, t denotes time and ν, k, and c_p respectively denote the fluid kinematic viscosity, thermal conductivity and specific heat at constant pressure. The viscous dissipation term $\rho_0 \nu e_{ij} e_{ij}$ is denoted by Φ, particle concentration by c and the infinitesimal rate-of-strain tensor by e_{ij}.

Although (2.1)–(2.3) are standard, more discussion is required concerning the particle concentration equation (2.4). We postpone this until a later section, and simply assume (a) that c evolves according to some linear operator $\mathcal{D}$ which will be specified later and (b) that the particle concentration does not appear in the flow and thermal equations.

To proceed, we non-dimensionalize (2.1)–(2.3). We set $x = L\bar{x}$, $y = L\bar{y}$, $z = \epsilon L\bar{z}$, $u = U\bar{u}$, $v = U\bar{v}$, $w = \epsilon U\bar{w}$, $t = (L/U)\bar{t}$, $p = (\rho_0 \nu U L/h_0^2)\bar{p}$ and $T = T_0 + (T_1 - T_0)\bar{T}$. Here $L(= 2a)$ and h_0 are respectively a typical length and height of the anterior chamber in a human eye and $\epsilon = h_0/L$. We assume also that U denotes a typical flow speed.

Dropping the bars for convenience, we find that

$$\epsilon^2 Re(u_t + uu_x + vu_y + wu_z) = -p_x + \epsilon^2(u_{xx} + u_{yy}) + u_{zz} + \epsilon^2 \frac{Re}{Fr}(1 - \alpha(T_1 - T_0)T) \tag{2.5}$$

$$\epsilon^2 Re(v_t + uv_x + vv_y + wv_z) = -p_y + \epsilon^2(v_{xx} + v_{yy}) + v_{zz} \tag{2.6}$$

$$\epsilon^2 Re(w_t + uw_x + vw_y + ww_z) = -\frac{p_z}{\epsilon^2} + \epsilon^2(w_{xx} + w_{yy}) + w_{zz} \tag{2.7}$$

$$u_x + v_y + w_x = 0 \tag{2.8}$$

$$T_t + uT_x + vT_y + wT_z = \frac{1}{RePr}\left(T_{xx} + T_{yy} + \frac{1}{\epsilon^2}T_{zz}\right) + \frac{Br}{\epsilon^2 RePr}(u_z^2 + v_z^2) \tag{2.9}$$

where the Reynolds, Prandtl, Froude and Brinkmann numbers are given respectively by

$$Re = \frac{LU}{\nu}, \quad Pr = \frac{\rho_0 \nu c_p}{k}, \quad Fr = \frac{U^2}{gL}, \quad Br = \frac{\rho_0 \nu U^2}{k(T_1 - T_0)} \tag{2.10}$$

and only the leading-order term in the viscous dissipation has been retained.

The non-dimensional parameters in (2.5)–(2.9) may now be estimated by using typical values for a human eye· using $h_0 = 2{\cdot}75\,\text{mm}$, $L = 11\,\text{mm}$, $U = 10^{-4}\,\text{m sec}^{-1}$ (an estimate based on observation that will be verified *a posteriori*), $\nu \sim 0{\cdot}9 \times 10^{-6}\,\text{m}^2\,\text{s}^{-1}$, $g = 9{\cdot}8\,\text{m s}^{-2}$ and $\alpha = 3 \times 10^{-4}\,\text{K}^{-1}$ we find that, as far as the momentum equations are concerned,

$$\epsilon^2 \sim 0{\cdot}06, \quad Re\epsilon^2 \sim 0{\cdot}076, \quad \epsilon^2 \frac{Re}{Fr}\alpha(T_1 - T_0) \sim 250(T_1 - T_0).$$

To lowest order, therefore, the traditional 'lubrication' assumptions are justified, and we note additionally that only very small temperature differences are required in order for the buoyancy forces to be strong enough to drive a non-trivial flow

The temperature equation may now be dealt with. We use standard thermal properties of water at blood temperature and assume that since the temperature changes involved are small, thermal properties may be regarded as being constant. We therefore use $\rho_0 = 10^3\,\text{kg m}^{-3}$, $c_p = 4{\cdot}2 \times 10^3\,\text{J kg}^{-1}\,\text{K}^{-1}$ and $k = 0{\cdot}57\,\text{W m}^{-1}\,\text{K}^{-1}$ (the thermal conductivity of human aqueous was measured by Poppendiek *et al.* (1966) who give a value of $k = 0{\cdot}578\,\text{W m}^{-1}\,\text{K}^{-1}$) giving

$$\frac{1}{RePr} \sim 0{\cdot}12, \quad \frac{1}{\epsilon^2 RePr} \sim 2, \quad \frac{Br}{\epsilon^2 RePr} \sim \frac{3 \times 10^{-11}}{T_1 - T_0}.$$

From this we conclude that the viscous dissipation may be ignored, and to leading order the temperature is governed by $T_{zz} = 0$. Of course, assuming (2.2) to be asymptotically large compared with (2.1) is dubious; almost certainly, however, this assumption will lead to results that are qualitatively correct. We therefore proceed on this basis If the convective terms in (2.9) were to be included, then matters would be complicated significantly. In particular, the x-momentum equation could no longer be solved in closed form and the whole problem would have to be attacked numerically Since we seek qualitative understanding of the flow we do not pursue this path

The final (redimensionalized) partial differential equations that we shall actually solve will therefore be

$$-\frac{p_x}{\rho_0} + \nu u_{zz} + g(1 - \alpha(T - T_0)) = 0 \tag{2.11}$$

$$-\frac{p_y}{\rho_0} + \nu v_{zz} = 0 \tag{2.12}$$

$$p_z = 0 \tag{2.13}$$

$$u_x + v_y + w_z = 0 \tag{2.14}$$

$$T_{zz} = 0. \tag{2.15}$$

The boundary conditions are no-slip ($u = v = w = 0$) on $z = h(x, y)$, $T = T_1$ on $z = 0$, $T = T_0$ on $z = h(x, y)$ together with conditions on the pressure at some point(s)

in the eye. Boundary conditions are also required for the velocity on $z = 0$, and these merit some discussion: although it would be simplest to treat the boundary $z = 0$ as a solid surface and impose a no-slip boundary condition there, under some circumstances this may not be valid. In the normal course of events fluid enters the anterior chamber through the pupil aperture and exits via the drainage angles at the boundaries of the cornea, the flow rates balancing each other so that the total amount of fluid in the anterior chamber remains constant. The fluid throughput is somewhat hard to ascertain, however. For the moment, therefore, we simply assume that on $z = 0$ we have $u = v = 0$ and $w = w_0(x, y)$ where $w_0(x, y)$ is assumed known.

In order to verify that the flow through the pupil aperture does not invalidate the lubrication assumptions, the order of magnitude of w_0 may be estimated by using the values given in Bill (1984). He quotes a typical uveoscleral outflow as $0{\cdot}5\,\mu\mathrm{l\,min^{-1}}$, asserting that this may account for up to 20% of the total vitreous body outflow. More recent measurements reported by Brubaker (1996) suggest that aqueous production is diurnal with an average value of $2{\cdot}3\,\mu\mathrm{l\,min^{-1}}$ (his specific measurements being $2{\cdot}91 \pm 0{\cdot}71\,\mu\mathrm{l\,min^{-1}}$ (08h00–12h00), $2{\cdot}66 \pm 0{\cdot}58\,\mu\mathrm{l\,min^{-1}}$ (12h00–16h00), and $1{\cdot}23 \pm 0{\cdot}41\,\mu\mathrm{l\,min^{-1}}$ (00h00–06h00)). Taking an estimated typical value of $2{\cdot}5\,\mu\mathrm{l\,min^{-1}} \sim 4{\cdot}2 \times 10^{-11}\,\mathrm{m^3\,s^{-1}}$ and a minimum pupil aperture radius of 1 mm leads to an average velocity of about $1{\cdot}3 \times 10^{-5}\,\mathrm{m\,s^{-1}}$. Comparing this with a typical $w = O(\epsilon U) \sim 2{\cdot}5 \times 10^{-5}\,\mathrm{m\,s^{-1}}$, it therefore seems likely that in all but the most extreme cases (for example, abnormally high aqueous production rates or very low temperature differences) (see Section 5) the flow through the pupil aperture will not contribute to leading order to the flow in the anterior chamber and use of the full no-slip condition on $z = 0$ is justified. Nevertheless, for the present we shall assume for the sake of completeness that w_0 is not zero.

Equations (2.11)–(2.15) may easily be solved. The temperature equation (2.15) yields

$$T = T_1 + \frac{z}{h}(T_0 - T_1)$$

and (2.11) thus becomes

$$0 = -\frac{p_x}{\rho_0} + \nu u_{zz} + g\,[1 - \alpha(T_1 - T_0)(1 - z/h)]$$

This equation may be integrated twice with respect to z, and, using the boundary conditions $u = 0$ on $z = 0$ and $z = h(x, y)$ we find that

$$u = \frac{p_x}{2\rho_0\nu}(z^2 - hz) + \frac{g}{\nu}\left[\frac{hz}{2} - \frac{z^2}{2} + \alpha(T_1 - T_0)\left(-\frac{hz}{3} + \frac{z^2}{2} - \frac{z^3}{6h}\right)\right] \tag{2.16}$$

Similarly we find that

$$v = \frac{p_y}{2\rho_0\nu}(z^2 - hz) \tag{2.17}$$

and

$$w = \frac{1}{2\rho_0\nu}\left[\left(\frac{hz^2}{2} - \frac{z^3}{3}\right)p_x\right]_x + \frac{1}{2\rho_0\nu}\left[\left(\frac{hz^2}{2} - \frac{z^3}{3}\right)p_y\right]_y - \frac{g\rho_0 z^2 h_x}{\rho_0\nu}\left[\frac{1}{4} + \frac{\alpha(T_1 - T_0)}{6}\left(\frac{z^2}{4h^2} - 1\right)\right] + w_0. \tag{2.18}$$

The pressure may now be determined by integrating the continuity equation from 0 to $h(x, y)$ with respect to z in the normal way· we find that

$$(h^3 p_x)_x + (h^3 p_y)_y = -12\rho_0\nu w_0 + \frac{g\rho_0}{2}[2 + \alpha(T_0 - T_1)](h^3)_x.$$

We assume that a pressure datum is fixed by setting $p = p_a$ say at $x = -a$. Then subtracting off the hydrostatic pressure, by setting

$$p = p_a + (x + a)g\rho_0\left[1 - \frac{\alpha(T_1 - T_0)}{2}\right] + P(x, y), \tag{2 19}$$

gives the equation for P as

$$(h^3 P_x)_x + (h^3 P_y)_y = -12\rho_0\nu w_o. \tag{2.20}$$

As we have seen, although the velocities have been determined for a general w_0 it is likely that in most instances the flow through the pupil aperture may be ignored. We therefore postpone consideration of non-zero w_0 until Section 5. With $w_0 = 0$ and $P = 0$ on the anterior chamber boundary we simply have $P = 0$ everywhere, so that, in the absence of any additional external mechanisms that might cause flow, the only important contribution to the pressure is hydrostatic. Thus

$$p = p_a + (x + a)g\rho_0\left[1 - \frac{\alpha(T_1 - T_0)}{2}\right].$$

The flow is essentially two-dimensional, the motion in each slice y = constant being independent of the flow in any other such cross-section and the overall flow being parametrized simply by $h(x, y)$. The velocities are given by

$$u = -\frac{(T_1 - T_0)g\alpha z}{12\nu h}(2z - h)(z - h) \tag{2.21}$$

$$v = 0 \tag{2.22}$$

$$w = -\frac{(T_1 - T_0)g\alpha z^2 h_x}{24\nu h^2}(z^2 - h^2) \tag{2.23}$$

and since $v = 0$ a stream function $\psi(x, y)$ (where as usual $u = \psi_z$, $w = -\psi_x$) may be introduced in the form

$$\psi = -\frac{(T_1 - T_0)g\alpha}{24\nu h} z^2(z - h)^2.$$

We may now examine the flow predicted by (2.21)–(2.23). We note first that for a given x, u is maximized with respect to z when

$$z = h(1/2 \pm \sqrt{3}/6) \sim 0{\cdot}21h, 0{\cdot}79h.$$

At this position

$$| u_{\max} | = \frac{(T_1 - T_0)g\alpha h^2\sqrt{3}}{216\nu}.$$

Using values of $g = 9{\cdot}8\,\mathrm{m\,s^{-2}}$, $\nu = 0{\cdot}9 \times 10^{-6}\,\mathrm{m^2\,s^{-1}}$, $h = 2{\cdot}75\,\mathrm{mm}$ and $\alpha = 3 \times 10^{-4}\,\mathrm{K^{-1}}$, we find that

$$u_{\max} \sim (T_1 - T_0)1{\cdot}98 \times 10^{-4}\,\mathrm{m\,s^{-1}\,K^{-1}}. \tag{2.24}$$

Alternatively, the average velocity (evaluated, say at $x = 0$) may be calculated, giving

$$| u |_{\mathrm{av}} = \frac{2}{h}\int_0^{h/2} | u | \,\mathrm{d}z = \frac{(T_1 - T_0)g\alpha h^2}{192\nu} \sim (T_1 - T_0)1{\cdot}29 \times 10^{-4}\,\mathrm{m\,s^{-1}\,K^{-1}}.$$

Each of these results seems to concur both with experimental and anecdotal observations and with our earlier non-dimensionalization.

Typical flow streamlines are shown in Fig. 4, where $h(x, y)$ was taken to be given (in non-dimensional form) by $h(x, y) = 1 - x^2 - y^2$. The streamlines along the slice $y = 0$ are much as expected, the flow rising against gravity near to the iris and falling with gravity towards the outside of the anterior chamber. It is worth remarking that detailed measurements of corneal shape have been made using a variety of experimental procedures (see, for example, Cho & Cheung, 2000, Schmid *et al.*, 2000, Diaz-Uribe & Granados-Agustin, 1999 and Vos *et al.*, 1997). The choice of corneal shape used in this study was made for simplicity, but the model could easily be changed to incorporate more complicated shapes if required.

Some further results of interest may be calculated now that the flow is essentially known: the shear stress on the boundary $z = 0$ is given by

$$\tau_0 = \rho_0\nu u_z(x, 0) = -\frac{(T_1 - T_0)g\alpha h(x, y)\rho_0}{12}$$

The negative sign occurs because the flow is opposing gravity near to the hotter internal wall of the anterior chamber. With the values used above we find that $\tau_0 \sim -6{\cdot}7 \times 10^{-4}(T_1 - T_0)\,\mathrm{kg\,m^{-1}\,s^{-2}\,K^{-1}}$. It is tempting to speculate that this might provide a mechanism for detaching more cells from the back of the anterior chamber of the eye, thereby potentially worsening the problem of eye drainage degradation. Previous studies of the role of fluid shear stress in detaching particles seem to suggest, however, that the stresses required to cause detachment are orders of magnitude larger than those predicted by our model. For example, Gerlach *et al.* (1997) observed endothelial cell detachment for shear stresses between $0{\cdot}51$ and $1\,53\,\mathrm{kg\,m^{-1}\,s^{-2}}$ and Vankooten *et al.* (1994) reported that the endothelial cell retention of glass reduced from 85% to 20% as the fluid shear stress increased from $8{\cdot}8$ to $26\,\mathrm{kg\,m^{-1}\,s^{-2}}$. We conclude that it is unlikely that anterior chamber flow plays a significant role in particle or cell detachment.

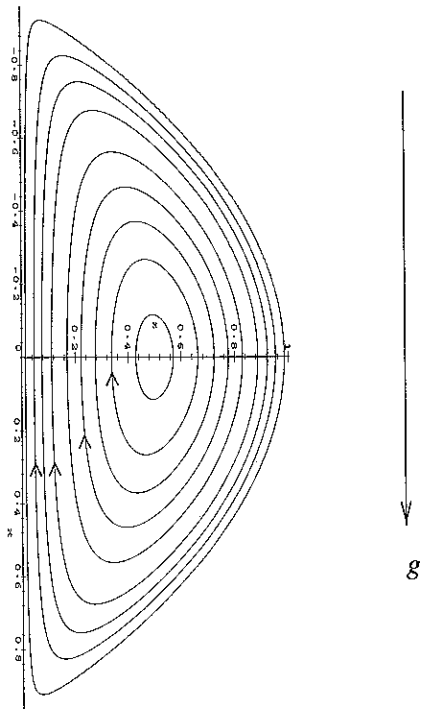

FIG 4. Typical streamlines for flow in the plane $y = 0$ within an anterior chamber with $w_0 = 0$.

It is also of interest to compare the flow-assisted transit time of a particle to the settling time if no convection were present. Suppose that a solid spherical particle of radius a_r, volume V_r, density ρ_r and mass m_r moves under gravity along the x-axis in an otherwise stationary flow. The Reynolds number Re_p based on a sphere radius $a_r = 5\,\mu$m and a flow speed of $U = 10^{-4}\,\mathrm{m\,s^{-1}}$ is given by

$$Re_p = \frac{a_r U}{\nu} \sim 6 \times 10^{-4},$$

and Stokes' drag law therefore applies. Thus

$$m_r \frac{\mathrm{d}^2 x}{\mathrm{d}t^2} = -6\pi\rho_0 \nu a_r \frac{\mathrm{d}x}{\mathrm{d}t} + V_r g(\rho_r - \rho)$$

where $x(t)$ denotes the vertical position of the particle. With $u = \mathrm{d}x/\mathrm{d}t$ and $x = u = 0$ at $t = 0$, we find that

$$x(t) = \frac{2a_r^2 g t(\rho_r - \rho_0)}{9\rho_0 \nu} + \frac{(\rho_0 - \rho_r) g a_r m_r}{27\pi\rho_0^2 \nu^2}\left[1 - \exp\left(\frac{-6\pi\rho_0 \nu a_r t}{m_r}\right)\right] \tag{2.25}$$

Using a particle density $1500\,\mathrm{kg\,m^{-3}}$ and a fluid viscosity of $\nu = 0{\cdot}9 \times 10^{-6}\,\mathrm{m^2\,s^{-1}}$, we find that the time taken for a particle to settle from the top to the bottom of the anterior

chamber (a distance of say 11 mm) is slightly in excess of 6 min. Comparing this to the transit time calculated using (2.24), which for a temperature difference of 3° K turns out to be about 18·5 s, we conclude that the presence of buoyancy-driven flow increases the effective mobility of particles in the flow by a factor of around 20. Although it is not obvious exactly how important a result this is (presumably there will be *some* flow in the eye anyway unless the patient is motionless for a long period of time), it seems that the case is clearly made that thermally driven flow is important as far as the creation of a hyphema or hypopyon is concerned.

3. The introduction of particulate matter into the flow

We now consider how particulate matter behaves when released into the flow Depending on their type and the circumstances that cause them to be present, particles may be released from the front of the iris, the pupil aperture, or at all locations on $z = 0$. We assume that such particles are then set free to move in the flow. In modelling the motion of such particles, we assume that they form a dilute mixture (so that they do not affect the fluid flow and particle–particle interactions are negligible) with a particle concentration by volume which we denote by c (a typical concentration is denoted by c_0). More sophisticated models could be proposed which treated the mixture as a two-phase flow; for this study, however, we ignore such complications.

It is now necessary to examine how the particles move in the flow. There are three sources of redistribution of such particles· diffusion, convection by the fluid flow as calculated above within the anterior chamber, and settling under gravity Balancing the Stokes drag for a constant settling velocity U_S against the buoyancy of a particle of density ρ_r gives

$$6\pi\rho_0\nu U_S a_r = \tfrac{4}{3}\pi(\rho_r - \rho_0)g a_r^3$$

and thus

$$U_S = \frac{2(\rho_r - \rho_0)g a_r^2}{9\rho_0\nu} \tag{3.1}$$

We may now determine whether or not the settling velocity is important; examining the ratio U_S/U for $U \sim 10^{-4}\ \mathrm{m\,s^{-1}}$ and particles of various sizes, we find that for particles of radius 4 μm

$$\frac{U_S}{U} \sim \frac{0{\cdot}4(\rho_r - \rho_0)}{\rho_0},$$

whilst for 0 5μm particles

$$\frac{U_S}{U} \sim \frac{6 \times 10^{-3}(\rho_r - \rho_0)}{\rho_0}.$$

We conclude that though in general the settling velocity must be retained in the problem, we may anticipate that pigment particles, on account of their much reduced size, are likely to behave in a manner rather different to that of red or white blood cells present in the anterior chamber.

Equation (3.1) determines U_S in terms of known particle properties, assuming sphericity, and will be used henceforth. It is worth pointing out, however, that if more information became available concerning the shapes of various particles, then (3.1) could easily be modified. For example, Pettyjohn & Christiansen (1948) recommend that for non-spherical particles the formula

$$U_S = \frac{2\kappa(\rho_r - \rho_0)g a_r^2}{9\rho_0 \nu}$$

is used, where a_r denotes the radius of a sphere of the same volume as the particle,

$$\kappa = 0{\cdot}843 \log_{10}(\psi_s/0{\cdot}065)$$

and ψ_S is the 'sphericity' of the particles (the ratio of the area of a sphere of the same volume as the particle to the area of the particle itself).

It is also appropriate to ask whether the use of a steady-state settling velocity is reasonable. To analyse the approach to terminal settling velocity we use (2.25), which shows that when a fraction λ of the terminal velocity $2(\rho_r - \rho_0)g a_r^2/9\rho_0\nu$ has been reached,

$$x = \frac{4a_r^4 \rho_r(\rho_r - \rho_0)g}{81\nu^2\rho_0^2}[-\lambda - \log(1-\lambda)].$$

For particles of radius 4μm and a density of $\rho_r = 2\rho_0$ say, and using standard values for water this predicts that 99% of terminal velocity will be reached after a distance of about 10^{-9} m, suggesting that the approximation involved in using the terminal settling velocity throughout will lead to negligible errors.

We may now propose a model for the evolution of particle concentration. The flux of particles $\boldsymbol{F}$ at any point is given by

$$\boldsymbol{F} = -D\nabla c + \boldsymbol{q}c + U_S c\hat{\boldsymbol{e}}_x$$

where D is the diffusion coefficient of particles in water and $\boldsymbol{q}$ is the fluid velocity given by (2.21)–(2.23). The particle concentration therefore satisfies

$$c_t + \operatorname{div}(-D\nabla c + \boldsymbol{q}c + U_S c\hat{\boldsymbol{e}}_x) = 0.$$

We non-dimensionalize using the same scalings employed previously along with $c = c_0\bar{c}$. Dropping the bars gives

$$c_t + uc_x + wc_z + \frac{U_S}{U}c_x = \frac{D}{\epsilon^2 UL}(\epsilon^2(c_{xx} + c_{yy}) + c_{zz}). \tag{3.2}$$

To estimate the sizes of the diffusion terms in (3.2) values are required for D. Complicated models based on Nernst–Einstein theory could be proposed for D and accurate values for this parameter will obviously be required if quantitative particle deposition rates are to be established. For the present, however, we postpone such complications and merely observe that for a very wide range of particles and solutions the diffusion coefficient in water is of

order $10^{-8} - 10^{-10}\,\mathrm{m^2\,s^{-1}}$ (see, for example, Lide, 1996). Thus (using $D = 10^{-9}\,\mathrm{m^2\,s^{-1}}$ and $U = 10^{-4}\mathrm{m\,s^{-1}}$)

$$\frac{D}{UL} \sim 10^{-3}, \quad \frac{D}{\epsilon^2 UL} \sim 0{\cdot}016.$$

The conclusions from this are much as one might expect: firstly, diffusion in the x- and y-directions may almost always be ignored (and will be henceforth in this study). Motion therefore still takes place in 'independent slices' $y =$ constant. The conclusions regarding diffusion in the z-direction are rather different; for although on time scales of the order of one transit (top to bottom of the anterior chamber) time (calculated below to be about 18 s) this effect may be ignored, for times of order hours (which are obviously clinically significant) and above, diffusion is important. The general picture is thus one of particles whose motion is dominated by a combination of settling and travel along streamlines, but which are slowly affected by diffusion which spreads them out into the centre of the anterior chamber.

The final (dimensional) partial differential equation to be solved is thus

$$c_t + (u + U_S)c_x + wc_z = Dc_{zz} \tag{3.3}$$

where u, v and U_S are given respectively by (2.21), (2.23) and (3.1).

Equation (3.3) requires boundary and initial conditions. (Though our main concern is to determine steady-state solutions, the numerical method that we will employ involves solving the unsteady problem.) We assume that $c = 0$ at $t = 0$ and set either $c = c_0$ (concentration given), $c_z = 0$ (zero flux) or $c_z = c_b$ (particle flux given) on the parts of the iris or pupil aperture which respectively do or do not produce particles.

On the cornea $z = h(x, y)$, we assume that particles may or may not adhere to each other and/or the surface of the cornea. For particles that do display a tendency to adhere, the flux of particles that adhere is assumed to be proportional to the concentration of particles already present. We therefore use the boundary condition

$$\boldsymbol{F}\cdot\hat{\boldsymbol{n}} = \sigma c \tag{3.4}$$

where $\hat{\boldsymbol{n}}$ is the unit outward-pointing normal to the cornea and σ may be regarded as an 'adherence' coefficient. In non-dimensional form, (3.4) becomes

$$(1 + \epsilon^2(h_x^2 + h_y^2))^{-1/2}[\epsilon^2 D(h_x c_x + h_y c_y) - \epsilon h_x h_0 U_S c - Dc_z] = \sigma c h_0. \tag{3.5}$$

When (3.2) was analysed, both of the terms U_S/U and $D/\epsilon^2 UL$ were retained; therefore (3.5) becomes

$$-\epsilon^2 L U_S h_x c - Dc_z = \sigma c h_0. \tag{3.6}$$

The final problem to be solved for the particle concentration c is therefore given by (3.3) with $c(x, y, z, 0) = 0$, either $c = c_0$ or $c_z = c_b$ (where c_b may be zero) on $z = 0$ and (3.6) on $z = h(x, y)$.

4. Numerical calculations of particle transport

We now seek to determine steady solutions to the particle concentration equation (3.3) using a realistic geometry and boundary conditions.

We note from (2.21) that u is zero on the anterior chamber centreline $z = h(x, y)/2$ as well as on $z = 0$ and at the cornea. This suggests performing a coordinate transformation in order to map the flow domain onto a computationally convenient region. We first non-dimensionalize the problem by setting $c = c_0\bar{c}$, $x = a(2\bar{x} - 1)$, $z = h_0\bar{z}$, $u = U\bar{u}$, $w = (h_0U/2a)\bar{w}$ and $t = (2a/U)\bar{t}$. Transforming from independent variables $(\bar{x}, \bar{z})$ to (X, Z) according to

$$X = \bar{x}, \qquad Z = \frac{2\bar{z}}{\bar{h}(\bar{x}, \bar{y})} - 1,$$

the problem to be solved becomes

$$\bar{c}_{\bar{t}} + \mathcal{U}\bar{c}_X + \mathcal{W}\bar{c}_Z = \frac{4\Gamma}{\bar{h}^2}\bar{c}_{ZZ} \tag{4.1}$$

where

$$\mathcal{U} = \lambda - A\bar{h}^2 Z(Z^2 - 1)$$

$$\mathcal{W} = \frac{3A}{4}\bar{h}\bar{h}_X(Z^2 - 1)^2 - \frac{\lambda\bar{h}_X}{\bar{h}}(1 + Z)$$

$$\Gamma = \frac{2aD}{Uh_0^2} \qquad A = \frac{(T_1 - T_0)g\alpha h_0^2}{48U\nu}, \qquad \lambda = \frac{U_S}{U}.$$

The boundary conditions are

$$\bar{c}(X, -1) = 1, \qquad \bar{c}_Z(X, -1) = 0, \quad \text{or} \quad \bar{c}_Z(X, -1) = \frac{\bar{h}c_b h_0}{2c_0}$$

whilst on the cornea we have

$$\bar{c}_Z(X, 1) = q_1\bar{c}(X, 1)$$

where

$$q_1 = \frac{\bar{h}h_0}{2D}\left(-\sigma - \frac{U_S h_o \bar{h}_X}{2a}\right).$$

A potential difficulty arises at the sides $X = 0$ and $X = 1$ of the transformed computational region. Since in general $h(x, y)$ is zero here, the diffusion term becomes unbounded in (4.1) and the standard numerical scheme described below cannot be applied. Moreover, since each of the boundaries $X = 0$ and $X = 1$ have finite length in the transformed

problem but represent the image of a point it is far from clear what the correct boundary conditions are. For elucidation, we examine (4.1) locally (near to $X = 0$, say). We have

$$\mathcal{U} \sim \lambda, \qquad \mathcal{W} \sim -\frac{\lambda(1+Z)\bar{h}_X}{\bar{h}}$$

and thus to leading order

$$\bar{c}_{ZZ} + \frac{\lambda(1+Z)\bar{h}\bar{h}_X}{4\Gamma}\bar{c}_Z = 0$$

Therefore locally

$$\bar{c} = A + B\,\mathrm{erf}\left[\sqrt{\frac{\lambda\bar{h}\bar{h}_X}{8\Gamma}}(1+Z)\right] \tag{4.2}$$

where A and B are constant. There are three separate boundary conditions on $Z = -1$ to consider, and three distinct cases of each, depending on whether $\bar{h}\bar{h}_X$ tends to 0, a constant or infinity as $X \to 0$. Since all computations (see below) will be carried out using $h(x, y) = h_0 - h_0(x^2 + y^2)/a^2$, we shall consider only the case where $\bar{h}\bar{h}_X \to 0$ (the others may be analysed similarly). In this instance (4.2) implies that $\bar{c} \sim A$, whilst to leading order the boundary condition on the cornea is $\bar{c}_Z = 0$. For the case where $\bar{c} = 1$ on $Z = -1$ we therefore set $\bar{c} = 1$ on the boundaries $X = 0$ and $X = 1$. Since $\bar{h}$ is zero at $X = 0$, the two cases where the boundary conditions at $Z = -1$ are $\bar{c}_Z(X, -1) = 0$ and $\bar{c}_Z(X, -1) = \bar{h}c_b h_0/2c_0$ are essentially the same. The conclusion is that it is not possible to determine the actual value of $\bar{c}$ in this case and instead $\bar{c}$ must be made continuous along $X = 0$ and $X = 1$ as Z goes from -1 to 1.

When y is non-zero, the model formulation is almost identical. If the equations are non-dimensionalized for a fixed y using $h_1 = h(0, y)$ instead of h_0 then we find that the problem to be solved is exactly the same as before, save for the fact that h_0 is replaced by h_1 in A, Γ, q_1 and c_b and a is replaced by the relevant semi-width in Γ and q_1.

4.1 *Numerical discretization*

We discretize the problem using a simple explicit method, differencing the convective terms according to the direction of the transport. For simplicity, we illustrate only the problem of calculating the flow in the slice $y = 0$. The region $0 \leqslant X \leqslant 1$, $-1 \leqslant Z \leqslant 1$ is divided into a rectangular mesh with increments $\delta X = 1/K$ and $\delta Z = 2/N$ say where K and N are the total number of mesh points in the X and Z directions respectively. We use a time step of size δt, and write $c^j_{k,n} = c(k\delta X, 0, -1 + k\delta Z, j\delta t)$. (The bars over non-dimensional variables have been dropped for convenience.) We begin by setting $c^j_{k,n} = 0$ at all internal mesh points, then advance in time until the concentration reaches a steady state.

For the main part of the flow where $1 \leqslant k \leqslant K - 1$ and $1 \leqslant n \leqslant N - 1$, (4.1) is differenced using the explicit finite-difference method

$$c^{j+1}_{k,n} = c^j_{k,n} - \frac{\delta t}{\delta X}(\mathcal{U}^+(c^j_{k,n} - c^j_{k-1,n}) + \mathcal{U}^-(c^j_{k+1,n} - c^j_{k,n}))$$

$$-\frac{\delta t}{\delta Z}(\mathcal{W}^+(c^j_{k,n}-c^j_{k,n-1})+\mathcal{W}^-(c^j_{k,n+1}-c^j_{k,n}))+\frac{4\Gamma\delta t}{h^2\delta Z^2}(c^j_{k,n+1}-2c^j_{k,n}+c^j_{k,n-1}) \tag{4.3}$$

where

$$\mathcal{U}^+=\begin{cases}\mathcal{U} & (\mathcal{U}\geqslant 0)\\ 0 & (\mathcal{U}<0)\end{cases},\qquad \mathcal{U}^-=\begin{cases}0 & (\mathcal{U}\geqslant 0)\\ \mathcal{U} & (\mathcal{U}<0)\end{cases}$$

and $\mathcal{W}^+$ and $\mathcal{W}^-$ are similarly defined.

At the top of the mesh, where $\mathcal{U}=\lambda$ and $\mathcal{W}=-2\lambda h_X/h$, the derivative boundary condition gives upon introducing the fictitious mesh points $c^j_{k,N+1}$ $(1\leqslant k\leqslant K-1)$

$$\frac{c^j_{k,N+1}-c^j_{k,N-1}}{2\delta Z}=q_1(X_k)c^j_{k,N}$$

Applying the difference scheme on $Z=1$ and eliminating the fictitious points therefore gives

$$c^{j+1}_{k,N}=c^j_{k,N}-\lambda\frac{\delta t}{\delta X}(c^j_{k,N}-c^j_{k-1,N})-\frac{\delta t}{\delta Z}(\mathcal{W}^+(c^j_{k,N}-c^j_{k,N-1})$$

$$+\mathcal{W}^-(c^j_{k,N-1}+(2\delta Zq_1(X_k)-1)c^j_{k,N}))+\frac{4\Gamma\delta t}{h^2\delta Z^2}(2c^j_{k,N-1}+2(\delta Zq_1(X_k)-1)c^j_{k,N}). \tag{4.4}$$

At the bottom of the mesh where $Z=-1$ the boundary conditions depend upon whether a mesh point corresponds to a location on the pupil aperture or the iris and what sort of concentration boundary condition is being assumed. At sites where it is assumed that $c=1$ the concentration value is known. At points where c_Z is known (whether it be zero or given say by F) we note that $\mathcal{U}=\lambda$, $\mathcal{W}=0$ and use fictitious mesh points in the normal way. Thus we have either

$$c^{j+1}_{k,0}=0 \tag{4.5}$$

or

$$c^{j+1}_{k,0}=c^j_{k,0}-\frac{\delta t}{\delta X}\lambda(c^j_{k,0}-c^j_{k-1,0})+\frac{4\Gamma\delta t}{h^2\delta Z^2}(2c^j_{k,1}-2c^j_{k,0}-hF\delta Z). \tag{4.6}$$

The condition at the sides of the mesh where $X=0$ and 1, depends, as discussed above, upon the boundary conditions being used on $Z=-1$. Since the differencing is explicit, when a Neumann boundary condition is imposed on $Z=-1$ we simply use a one-sided difference. Thus for $1\leqslant n\leqslant N-1$ we impose

$$\text{(Dirichlet condition on } Z=-1\text{):}\quad c^{j+1}_{0,n}=c^{j+1}_{K,n}=1 \tag{4.7}$$

$$\text{(Neumann condition on } Z=-1\text{):}\quad c^{j+1}_{0,n}=c^{j+1}_{1,n},\quad c^{j+1}_{K,n}=c^{j+1}_{K-1,n} \tag{4.8}$$

The conditions for numerical stability of the simple numerical scheme (4.3)–(4.5) or (4.6) and (4.7) or (4.8) may either be established directly using standard means or by making some obvious simple modifications to analyses for standard schemes. Using, for example, an obvious generalization to the result presented in Roach (1976), we find that for stability the time step δt must satisfy

$$\delta t \leqslant \frac{1}{\dfrac{8\Gamma}{h_m^2 \delta Z^2} + \dfrac{u_m}{\delta X} + \dfrac{w_m}{\delta Z}}$$

where

$$h_m = \min \mid h(X, Y) \mid, \qquad u_m = \max \mid u(X, Y) \mid, \qquad w_m = \max \mid w(X, Y) \mid .$$

Since u, w and h are known before the computations are started, this requirement is easily implemented. It is easily confirmed that the theoretical stability requirement is well borne out in practice.

Coding was carried out in FORTRAN 77 on a P200 running Linux. In all computations a time step of 0.95 times the theoretical maximum time step was used and a (dimensional) corneal shape

$$h(x, y) = h_0(1 - r^2/a^2)$$

was assumed.

4.2 *Hyphema formation*

Typical numerical results for the formation of a hyphema are shown in Fig. 5. A 41×41 grid was used to produce these results, which were calculated at 45 cross-sections of the anterior chamber. A diffusion coefficient $D = 10^{-8}\,\mathrm{m^2\,s^{-1}}$ was used and red blood cells of diameter $3{\cdot}5\,\mu\mathrm{m}$ and density $1500\,\mathrm{kg\,m^{-3}}$ were assumed to enter from the whole of the base of the chamber. The adherence coefficient σ was chosen to be zero, reflecting the fact that red blood cells are largely unsticky. The buoyancy constant A was taken to be 10, implying a temperature difference between the front and rear of the anterior chamber of about 2° C. The calculations also used $h_0 = 2.75\,\mathrm{mm}$, whilst the chamber and pupil radii were taken to be 5.5 mm and 2.25 mm respectively. Using $\rho_0 = 1000\,\mathrm{kg\,m^{-3}}$, $g = 9{\cdot}8\,\mathrm{m\,s^{-2}}$ and $\nu = 0{\cdot}9 \times 10^{-6}\,\mathrm{kg\,m^{-1}\,s^{-1}}$ gave a settling velocity of $U_S = 1{\cdot}48 \times 10^{-5}\,\mathrm{m\,s^{-1}}$. A typical time step for the calculation was about 10^{-5} in non-dimensional time units and most cases required order 3×10^5 iterations to converge.

Two views are shown. The upper half of the figure shows a head-on view of the anterior chamber. Particle concentration increases as the colour changes from dark blue through green, yellow and orange to red; the dark red region indicates the area of maximum red blood cell concentration. The overall impression is very similar to what one sees in the eye of a patient with a hyphema. In the lower half of the figure the same colour scheme is used to indicate red blood cell concentration in a slice taken through the anterior chamber at $y = 0$. We see that over most of the chamber particle concentration is relatively low, but there is a sudden rise near the base of the chamber which gives a characteristic hyphema

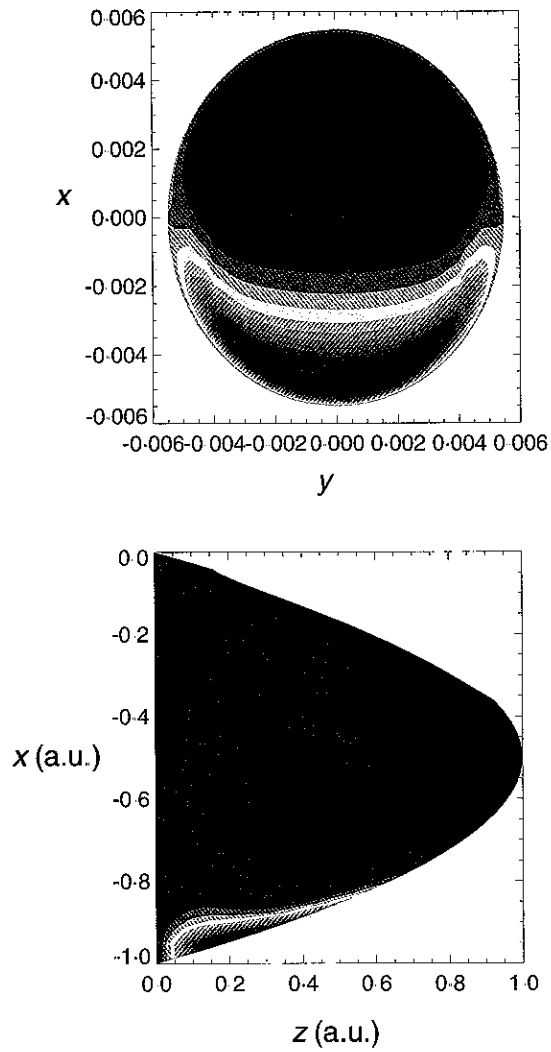

FIG 5. Numerical results for hyphema formation. Top: view from front of concentration on cornea. Bottom: side view of slice $y = 0$ (concentration increases from dark blue through green, yellow and red to dark red). Note: in the bottom view the very high concentration gradient around the upper corneal surface is not resolved perfectly in the figure.

shape. The effects of the buoyancy-driven circulation are also apparent in the lower view. We carried out a number of numerical tests with other parameter values; in each one similar pictures were produced.

Though we have not included hypopyon predictions in the current study, it is evident that the necessary calculations would proceed along similar lines, and, owing to the similar properties of white and red cells, yield similar results. To predict keratic precipitates would also be possible, though some submodel would have to be adopted to deal with particle clumping.

4.3 *Flow-induced hyphema disruption*

Using the model described above, some simple estimates may be made of the maximum possible size of a hyphema for given parameter values. We suppose that a hyphema has formed at the base of the cornea and ask how far it can project upwards into the flow before its constituent red blood cells can overcome the force of gravity and be swept away into the flow. Assuming that the red blood cells have radius a_r, density ρ_r and are subject to Stokes' drag, the condition that the settling force is overcome by the convective flow is given by

$$-6\pi\rho_0 v u a_r > V_r g(\rho_r - \rho_0)$$

where V_r is the volume of a red blood cell. Using (2.21), this gives

$$\frac{\rho_0\pi(T_1 - T_0)a_r\alpha g z(2z - h)(z - h)}{2h} > \frac{4}{3}\pi a_r^3(\rho_r - \rho_0)g,$$

which may be simplified to

$$z(2z - h)(z - h) > \frac{8ha_r^2(\rho_r - \rho_0)}{3\alpha(T_1 - T_0)\rho_0}.$$

We note that for $h/2 < z < h$ a hyphema can never be disrupted as the flow is in the same direction as gravity. Particles, however, at say $z = \lambda h$ where $0 < \lambda < 1/2$, will overcome gravity-induced settling so long as

$$h^2\lambda(1 - 2\lambda)(1 - \lambda) > \frac{8a_r^2(\rho_r - \rho_0)}{3\alpha(T_1 - T_0)\rho_0}. \tag{4.9}$$

Particles in a hyphema may therefore move most easily when $\lambda(2\lambda - 1)(\lambda - 1)$ attains a maximum, which occurs at $\lambda = 1/2 - \sqrt{3}/6 \sim 0{\cdot}211$. Using this value of λ in (4.9) and simplifying, we find that a hyphema can exist only where the corneal height h satisfies

$$h^2 \leqslant \frac{16\sqrt{3}a_r^2(\rho_r - \rho_0)}{\alpha(T_1 - T_0)\rho_0}.$$

Using $a_r = 3{\cdot}5\,\mu\text{m}$, $\rho_r = 1500\,\text{kg m}^{-3}$, $\rho_0 = 1000\,\text{kg m}^{-3}$ and $\alpha = 3 \times 10^{-4}\,\text{K}^{-1}$ now gives a critical corneal height (measured in m) of

$$h \leqslant \frac{k_1}{\sqrt{T_1 - T_0}}$$

where $k_1 = 7{\cdot}5 \times 10^{-4}\,\text{mK}^{1/2}$, which seems well in accordance with observation.

In addition to suggesting that the mathematical model predicts very plausible maximum sizes for hyphemas, the above results suggest a speculative treatment for the dispersion (or at least amelioration) of a hyphema. Since the size of the hyphema has been seen to depend inversely upon the square root of the temperature difference from the cornea to the pupil and iris, a cold eye patch worn by the patient is likely to decrease hyphema size and provide a temporary treatment for this condition. Thus far, we have been able to find

no details in the literature of such a procedure being used, though the use of cold jets on the eye to promote natural convection and to consequently enhance mixing of various pharmacological agents has been previously employed (see, for example, Kaufman, 1985 and Gabelt *et al.*, 1991). An ethically acceptable experimental study could easily be designed: its main component would involve observational studies of the movement of particles in an anterior chamber (i) during the day (ii) at say 3.00am immediately after awakening from sleep, (iii) several hours after a double eye-pad has been applied and (iv) after application of an ice-pack. This would involve only minor inconvenience and virtually no discomfort for the patient. We are hoping to proceed with such a study in the near future.

5. The formation of a Krukenberg spindle

We now examine the formation of a Krukenberg spindle. The distinguishing feature of a Krukenberg spindle is that it is formed by pigment particles which are so light and small that their settling velocity is negligible. It therefore seems that that the formation of such deposits must *perforce* involve flow into and out of the anterior chamber. Anecdotal evidence suggests that the formation of a Krukenberg spindle may take place mainly during sleep. We hypothesize that pigment particles are 'generated' during waking hours by a 'reverse pupil block' mechanism (see, for example, Ball, 1999) involving increased contact between the iris and the anterior lens surface. At night, a patient's closed eyelids effectively insulate the anterior chamber. Further temperature equalization is provided by the fact that ambient conditions tend to be warmer than during the day and no tear evaporation takes place. The thermal gradient across the anterior chamber is thus greatly reduced and may vanish completely. The effects of buoyancy and gravity (whose effective direction is dictated by the patient's sleeping position) are therefore negligible and flow is dominated by fluid motion through the pupil aperture. We therefore consider the case $w_0 \neq 0$. If we write (2.20) in polar coordinates as

$$\frac{1}{r}(rh^3P_r)_r + \frac{1}{r^2}(h^3P_\theta)_\theta = -12\rho_0\nu w_0$$

then for general h it is clear that a numerical solution will be required. If, however, we assume that both the eye geometry and the inflow are symmetrical so that h and w_0 depend only upon r, the pressure equation may be solved to yield

$$P = -12\rho_0\nu\Omega(r) + \text{constant}$$

where $\Omega(r)$ satisfies

$$\frac{(rh^3\Omega_r)_r}{r} = w_0$$

and the constant of integration is chosen to ensure that $P = 0$ when $h = 0$. For a given h and w_0 the solution for the flow is now completely determined.

A simple example of the sort of flow that might be expected is furnished by taking

$$w_0 = A_1(r^2 - a^2)(r^2 - a^2/3), \qquad h = h_0\sqrt{1 - r^2/a^2} \tag{5.1}$$

where A_i, (which characterizes the injection rate) and h_0 are suitably chosen constants. The inflow/outflow velocity distribution $w_0(r)$ has been chosen so that the total amount of fluid in the anterior chamber remains constant; it is also passably realistic in that it simulates inflow through a pupil aperture (of radius $a/\sqrt{3}$) and outflow concentrated over a fairly small region near to $r = a$. (It is worth mentioning that it is in fact possible to refine the choice for w_0 to include delta-function type behaviour at the angles for increased realism; the results are very similar however, and the mathematics is greatly complicated.) Using (5.1) gives

$$P = \frac{2A_i\rho_0\nu a^3}{3h_0^3}(a^2 - r^2)^{3/2} \tag{5.2}$$

and the complete velocity distribution is now determined. In its most general form, the flow is fully three-dimensional, the effects of buoyancy competing with those of flow through the pupil aperture. For small values of A_i, the incoming flow makes little difference and the flow is very similar to that shown in Fig. 4. When A_i is taken to be so large that the injection dominates the flow, then the result is an axisymmetric flow with almost no θ-dependence; the flow streamlines rise from the pupil aperture, bend around below the cornea, and exit via the iris. It is worth examining this latter case in a little more detail, for, as explained above, the results lead one to speculate that a Krukenberg spindle is formed under circumstances when buoyancy forces are negligible. When A_i is large the flow is given essentially by

$$u = \frac{a^3A_ixz}{h_0^3}(h_0\sqrt{1 - r^2/a^2} - z)(a^2 - r^2)^{1/2} \tag{5.3}$$

$$v = \frac{a^3A_iyz}{h_0^3}(h_0\sqrt{1 - r^2/a^2} - z)(a^2 - r^2)^{1/2} \tag{5.4}$$

$$w = \frac{a^3A_i}{h_0^3}\left[\frac{z^3(2a^2 - 3r^2)}{3\sqrt{a^2 - r^2}} - \frac{h_0z^2(a^2 - 2r^2)}{a} + \frac{h_0^3(a^2 - r^2)(a^2 - 3r^2)}{3a^3}\right]. \tag{5.5}$$

Figure 6 shows streamlines for this flow in a slice $y = 0$ of the anterior chamber. (Note that the Reynolds number based on w_0 at $r = 0$ and an aperture radius of $a/\sqrt{3}$ is given by $(A_ia^5)/(3\sqrt{3}\nu)$ which, with $A_i = 10^4\,s^{-1}\,m^{-3}$, $a = 6{\cdot}5$ mm and $\nu = 0{\cdot}9 \times 10^{-6}\,m^2\,s^{-1}$ gives about 0 025, so that the assumption of slow flow is valid.) For a Krukenberg spindle to form, it is clear that (a) particles must be convected close to the cornea by the flow and (b) particles must have some chance to adhere to the cornea. The former condition depends simply on which streamline the particles are injected. We may expect that whether or not the latter condition is satisfied will depend largely on the amount of shear stress that the flow exerts on a particle. To leading order, the magnitude of the shear stress on the cornea is given by $\tau_c = |\,(\rho_0\nu u_z, \rho_0\nu v_z, 0)\,|_{z=h(x,y)}$. Thus

$$\tau_c = -\frac{\rho_0\nu A_ia^2}{h_0^2}r(a^2 - r^2).$$

We therefore seek to generate a Krukenberg spindle in the anterior chamber as follows: we numerically generate particles at random locations in the pupil aperture and follow

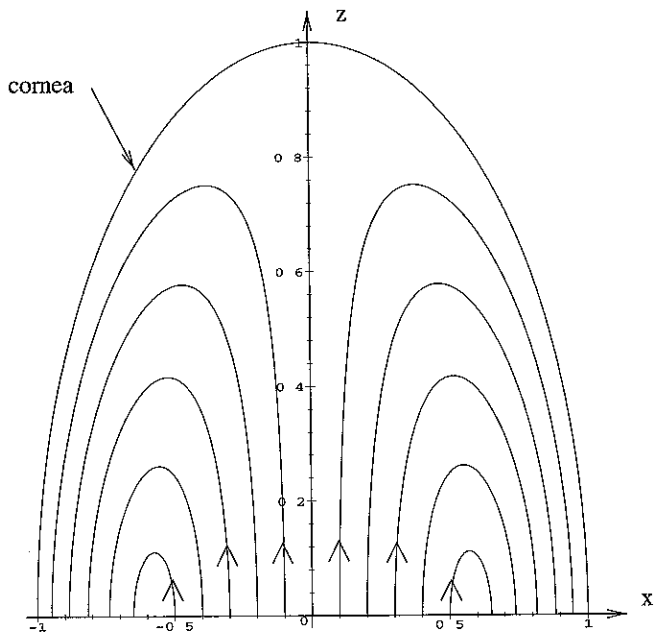

FIG 6. Streamlines in slice $y = 0$ of anterior chamber for flow through pupil aperture.

their progress along the flow streamlines by solving $dx/dt = u$, $dy/dt = v$ and $dz/dt = w$ (where u, v and w are given by (5.3)–(5.5)) using a standard numerical initial value problem solver. Pigment particles are then adjudged to have 'stuck' to the cornea so long as (a) they approach to within a specified distance of the cornea and (b) the corneal shear stress at the sticking point is less than a given value. Figure 7 shows a Krukenberg spindle generated in just such a manner: a value of $A_i = 10000\,s^{-1}\,m^{-3}$ (which corresponds to a flow rate through the pupil aperture of about $2{\cdot}5\mu l\,min^{-1}$) was used for the computations. Of the 5000 particles generated, 399 stuck to the cornea and 4601 eventually exited the anterior chamber.

Although our main objectives of providing mechanisms and predictions for hyphema and Krukenberg spindle formation have now been achieved, it is worth noting that when the effects of injection and buoyancy compete the flow is fully three-dimensional and the exact solution given by (2.16)–(2.18), (2.19), (5.1) and (5.2) is of fluid dynamical interest in its own right. Although space constraints permit only the briefest discussion of such flows, we note some of the more important details. The top portion of Fig. 8 shows particle paths in the plane $y = 0$ for parameter values $a = 5{\cdot}5\,mm$, $h_0 = 2{\cdot}75\,mm$, $g = 9\,8\,m\,s^{-2}$, $\nu = 0{\cdot}9 \times 10^{-6}\,m^2\,s^{-1}$, $\rho_0 = 1000\,kg\,m^{-3}$, $\alpha = 3 \times 10^{-4}\,K^{-1}$ and $A_i = 10^4\,sec^{-1}\,m^{-3}$. The temperature difference in this case was taken to be $T_1 - T_0 = 0{\cdot}02°$ C. Fluid enters the anterior chamber from the pupil aperture and some exits as might be expected near to the corners of the chamber. We note, however, that a stagnation point exists in the flow (located at $x \simeq 2{\cdot}4\,mm$, $y \simeq 1\,mm$) and captures fluid that enters from some parts of the pupil aperture. Although this seems to violate conservation of mass, it may be confirmed that the

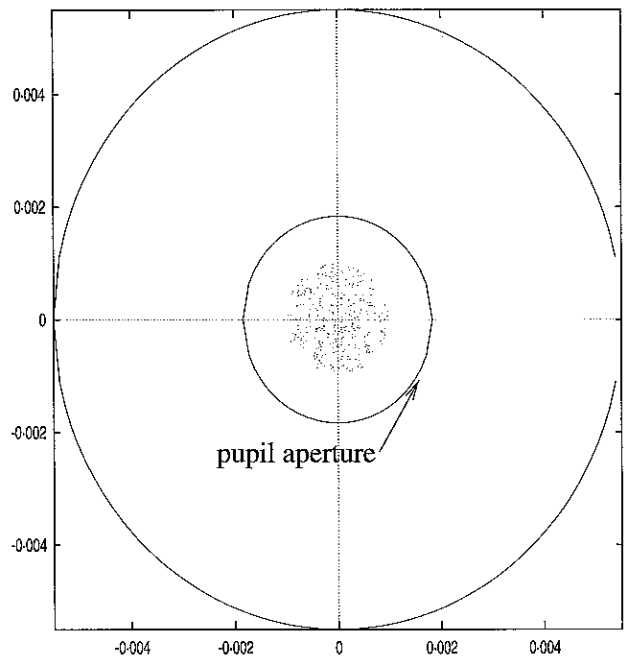

FIG 7 Numerical simulation of Krukenberg spindle formation resulting from flow through pupil aperture.

stagnation point is two-dimensional and thus 'traps' only fluid particles that originate from the plane $y = 0$.

Examination of the particle paths of fluid particles that originate from locations near to the plane $y = 0$ confirm that the flow streamlines look largely like those in Fig. 8. During the final approach to the stagnation point, however, such particles are ejected normal to the plane $y = 0$· for example, fluid particles originating from $x = 1$ mm, $y = 0{\cdot}01$ mm, $z = 0$ eventually exit the anterior chamber at $x = -1{\cdot}07$ mm, $y = 3{\cdot}98$ mm, $z = 0$. The complete three-dimensional flow pattern is thus extremely complicated and almost impossible to display successfully in two dimensions.

6. Discussion and conclusions

A simple model has been developed which predicts the details of thermally driven flow in the anterior chamber of the eye. Although historically there has been little doubt that such flows really exist, unless particles are present in the anterior chamber it is extremely difficult to observe fluid motion and some previous discussions have relied upon anecdotal evidence The model presented above shows unequivocally that buoyancy driven flows in the anterior chamber are inevitable, and indicates that only very small temperature differences are required to drive such flows. Wyatt (1996) remarks that (apart from cooling currents in the inner ear that are believed to lead to dizziness) there seem to be no other circumstances in the healthy human body where natural convection plays a significant role.

In Section 3 the effect of adding particulate matter to the flow was discussed. Such

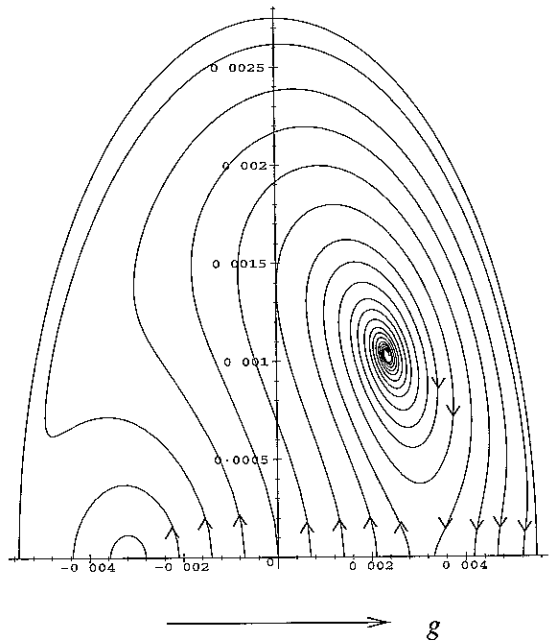

FIG. 8. Particle paths for flow in the plane $y = 0$ when the effects of buoyancy and flow through the pupil aperture have equal importance.

particulate matter may be present as the result of eye trauma or as a by-product of a range of conditions and diseases that may affect the eye. Analysis of the equations shows that thermally driven flow provides a powerful mechanism for the distribution of particles within the anterior chamber that may compete with gravity-induced settling to determine the final distribution of red, white or pigment cells in the anterior chamber.

Our predictions of Krukenberg spindle formation concur in their general features with what is observed by eye surgeons (though many different shapes of spindle are observed). It is possible, however, that, after nocturnal formation, the structure may be smeared somewhat by particles sliding under the action of buoyancy-driven convection during the day. Some (rather inconclusive) evidence suggests that although this may be the case, the smearing only takes place in the direction of gravity; this again accords well with the theory presented above and would give rise to the 'spindle' shape that is most often seen.

Because our aim in this study was to use asymptotic analysis to gain a qualitative understanding of the flow, many simplifications have been made. In particular, the ability of the particles to adhere to one another (especially important in the case of white blood cells) was not considered, whilst the tendency of particles to stick to the surface of the cornea was modelled in the simplest possible way. The full details of the deposition and resuspension of particles in a flow are extremely complicated (see, for example, Please & Wilmott, 1987) and much more complicated modelling would be required if this matter was to be addressed in detail. Future models should also give more attention to the way in which particulate matter is released and enters into the flow. One problem in adopting refined modelling of

this sort would be to adequately compare putative models to observed behaviour. Evidently ethical considerations dictate that the sort of detailed *in vivo* experiments that would be required to validate detailed particle release and corneal adherence models would be fraught with difficulty.

Another area in which more detailed study might be possible concerns the heat transfer across the cornea. We have assumed simply that the temperature on the inside of the cornea takes some given value, which is lower than body temperature. In reality, one might expect that the ambient temperature would be attained on the corneal epithelium rather than, as assumed, to the endothelium. Although our analysis has shown conclusively that only very small temperature gradients are required to drive a flow, at present we have no means of estimating how large these differences might actually be (other than comparing observed particle transit times with those predicted for a given temperature difference by say (2.21) and (2.23)). Although this might be a fertile area for future research, it is not a simple one; matters are complicated by motion of the eye and eyelid, and the fact that the corneal surface is continually bathed by tear film which flows and evaporates. We have, however, carried out some parametric studies using a Newton cooling boundary condition at the corneal surface, assuming that the thermal properties of corneal tissue are similar to those of water (see, for example, ICRP, 1975) and incorporating various different forms of heat transfer coefficient. As might be expected, inclusion of these effects made very little difference to any of the results.

It is also worth mentioning that other mechanisms (for example, changes in the pupillary diameter and extraocular muscle-induced motion of the eyes) might enhance particle transport. Though these are primarily unsteady effects, their influence could be added to more detailed models of the flow

One of the more important by-products of the model developed above is the identification of important non-dimensional parameters in the problem. The ability to characterize the strength of thermally induced buoyant convection suggests a method for assisting the process of hyphema break-up. For example, applying a cooled eye patch would increase the temperature difference across the anterior chamber. This should increase convection and disperse the hyphema. As far as the authors are aware this is a new idea. It seems, however, that since the possible benefits of such treatment are great whilst the side effects seem to amount to no more than some temporary mild discomfort, the treatment could be tested with few attendant risks.

Acknowledgements

The authors are grateful to Colin Please and Adam Wheeler (Faculty of Mathematical Studies, University of Southampton), Kerry Landman (Department of Mathematics and Statistics, University of Melbourne, Victoria, Australia), Robert Maclaren (Merton College, Oxford) and Harry Wyatt (Schnurmacher Institute for Vision Research, SUNY, New York USA) for their contributions to informal discussions concerning the mathematical modelling of this problem.

REFERENCES

BALL, S. F. (1999) Pigmentary glaucoma. *Ophthalmology.* (M. Yanoff & J. S. Duker, eds) London: Mosty.

BATCHELOR, G K. (1985) *An Introduction to Fluid Dynamics* Cambridge: Cambridge University Press.

BILL, A (1984) Physiology of the outflow mechanism. *Applied pharmacology in the medical treatment of glaucomas* (S M Drance, ed.). Orlando: Grune & Stratton.

BRUBAKER, R. F. (1996) Measurement of aqueous flow by fluorophotometry. *The Glaucomas, 2nd Edition.* (R. Ritch, M. B Shields & T Krupin, eds). St. Louis, MO: Mosty

CARO, C. G., PEDLEY, T. J., SCHROTER, R C & SEED, W. A (1978) *The Mechanics of Circulation.* Oxford: Oxford University Press.

CHO, P. & CHEUNG, S W (2000) Central and peripheral corneal thickness measured with the TOPCON specular microscope. *Curr. Eye Res.*, **21**, 799–807

CRAMER, R., DRI, P , ZABUCCHI, G. & PATRIARCA, P (1992) A simple and rapid method for isolation of eosinophilic granulocytes from human blood. *J. Leukocyte Bio.*, **52**, 331–336.

DIAZ-URIBE, R. & GRANADOS-AGUSTIN, F. (1999) Corneal shape evaluation using laser keratopography. *Optometry Vis. Sci.*, **76**, 40–49

DRAZIN, P. G. & REID, W H (1981) *Hydrodynamic Stability* Cambridge: Cambridge University Press.

DUCK, F. A. (1990) *Physical Properties of Tissue.* London: Academic.

EHRLICH, P (1882) Über provocirte Fluorescenzerscheinungen am Auge. *Deutsch. med. Wschr.*, **8**, 35–37.

FARRAR, S M. & SHIELDS, M. B. (1993) Current concepts in pigmentary glaucoma. *Surv. Ophthalmol.*, **37**, 233–252.

FATT, I. & WEISSMAN, B A. (1992) *Physiology of the Eye: an Introduction to the Vegetative Functions - 2nd Edition* New York: Butterworth-Heinemann.

GABELT, B T , CRAWFORD, K. & KAUFMAN, P L (1991) Outflow facility and its response to pilocarpine decline in aging rhesus-monkeys *Arch. Ophthalmol.*, **109**, 879–882

GERLACH, J C., HENTSCHEL, F., SPATKOWSKI, G., ZEILINGER, K , SMITH, M. D & NEUHAUS, P (1997) Cell detachment during sinusoidal reperfusion after liver preservation—An in vitro model. *Transplantation*, **64**, 907–912.

ICRP (INTERNATIONAL COMMISSION ON RADIOLOGICAL PROTECTION), (1975) *Report of the Task Group on Reference Man, ICRP Publication 23* Oxford: Pergamon.

KAUFMAN, P L (1985) Isoproteronel dose-outflow facility response relationships in the vervet monkey. *Curr. Eye Res* , **4**, 877–883

KRUKENBERG, F (1899) Beiderseitige angeborene Melanose der Hornhaut. *Klin. Mbl. Augenheilk.*, **37**, 254–258.

KUCHLE, M , MARDIN, C Y., NGUYEN, N. X., MARTUS, P. & NAUMANN, G O. H (1998) Quantification of aqueous melanin granules in primary pigment dispersion syndrome. *Am. J. Ophthalmol.*, **126**, 425–431.

LIDE, D. R (Ed.) (1996) *CRC Handbook of Chemistry and Physics, 77th Edn.*. Boca Raton, FL: CRC Press

LURIE, S (1992) Density distribution of erythrocyte population in preeclampsia. *Gynecol. Obstet. Inves.*, **33**, 94–97

PETTYJOHN, E S. & CHRISTIANSEN, E B (1948) Effects of particle shape on free settling rates of isometric particles. *Chem. Eng. Prog.*, **44**, 157–172.

PLEASE, C P. & WILMOTT, P. (1987) The deposition and resuspension of small radioactive particles in a recirculating flow in a reactor *Math. Engng Ind.*, **1**, 21–32.

POPPENDIEK, H F., RANDELL, R , BREEDEN, J. A., CHAMBERS, J E. & MURPHY, J R. (1966) Thermal conductivity measurements and predictions for biological fluids and tissues *Cryobiology*, **3**, 318–327.

ROACH, P. J. (1976) *Computational Fluid Dynamics*. Albuquerque, New Mexico: Hermosa.

SCHMID, G., PETRIG, B., RIVA, C, LOGEAN, E & WALTI, R (2000) Measurement of eye length and eye shape by optical low coherence reflectometry *Klin. Mbl. Augenheilk.*, **216**, 324–326.

SEELEY, R. R., STEPHENS, T. D & TATE, P (2000) *Anatomy & Physiology, 5th Edn.*. New York: McGraw–Hill.

TÜRK, S. (1906) Untersuchungen über eine Strömung in der vorderen Augenkammer. *von Graefes Arch. Ophthalmol.*, **64**, 481–501.

TÜRK, S. (1911) Weitere Untersuchungen über Wärmeströmung in der vorderen Augenkammer und die Ehrlichsche Linie. *Klin. Mbl. Augenheilk.*, **49**, 300–321.

VANKOOTEN, T G, SCHAKENRAAD, J. M., VANDERMEI, H C., DEKKER, A., KIRKPARTICK, C. J. & BUSSCHER, H J (1994) Fluid shear–induced endothelial–cell detachment from glass–influence of adhesion time and shear–stress. *Med. Eng. Phys.*, **16**, 506–512.

VOS, F. M, VANDERHEIJDE, R G. L., SPOELDER, H J W., VANSTOKKUM, I. H M. & GROEN, F. C A. (1997) A new instrument to measure the shape of the cornea based on pseudorandom color coding. *IEEE Trans. Instrum. Meas*, **46**, 794–797.

WEATHERALL, D J., LEDINGHAM, J. G. G & WARRELL, D. A. (1996) *Oxford Textbook of Medicine - 3rd Edn.* Oxford: Oxford University Press.

WYATT, H. J. (1996) Ocular pharmacokinetics and convectional flow: evidence from spatio–temporal analysis of mydriasis. *J Oc. Pharm. Thera.*, **12**, 441–459.